arXiv:cond-mat/9808073v1 7 Aug 1998

Kinetics of four-wave mixing for a 2D magneto-plasma in strong magnetic fields

M. W. Wu and H. Haug
Institut für Theoretische Physik, J.W. Goethe Universität Frankfurt, Robert-Mayer-Straße 8, D-60054 Frankfurt a. M., Germany
(February 1, 2008; E-mail: wu@mandala.th.physik.uni-frankfurt.de)

We investigate the femtosecond kinetics of an optically excited 2D magneto-plasma at intermediate and high densities under a strong magnetic field perpendicular to the quantum well (QW). We assume an additional weak lateral confinement which lifts the degeneracy of the Landau levels partially. We calculate the femtosecond dephasing and relaxation kinetics of the laser pulse excited magneto-plasma due to bare Coulomb potential scattering, because screening is under these conditions of minor importance. In particular the time-resolved and time-integrated four-wave mixing (FWM) signals are calculated by taking into account three Landau subbands in both the valance and the conduction band assuming an electron-hole symmetry. The FWM signals exhibit quantum beats mainly with twice the cyclotron frequency. Contrary to general expectations, we find no pronounced slowing down of the dephasing with increasing magnetic field. On the contrary, one obtains a decreasing dephasing time because of the increase of the Coulomb matrix elements and the number of states in a given Landau subband. In the situation when the loss of scattering channels exceeds these increasing effects, one gets a slight increase at the dephasing time. However, details of the strongly modulated scattering kinetics depend sensitively on the detuning, the plasma density, and the spectral pulse width relative to the cyclotron frequency.

42.50.Md, 42.65.Re, 42.50.-P, 78.47.+p

I. INTRODUCTION

Femtosecond pulse excitation in semiconductors induces transient carrier populations, which can be studied through ultrashort-pulse nonlinear optics to elucidate many-body effects, such as time-dependent Coulomb correlations. Numerous experimental and theoretical studies have been devoted to this problem in the magnetic-field-free case in the last ten years.[1–3] Studies of femtosecond laser spectroscopy in the presence of a strong magnetic field are relatively rare and are mainly focused on magneto-excitons at low excitation densities[4–6,13]. For a strong resonant laser pulse which excites an electron-hole (e-h) system with a density above the Mott ionization density, the kinetics is dominated by Coulomb scattering in the correlated e-h plasma or in the correlated magneto-plasma if a strong magnetic field is present. The femtosecond quantum kinetics and the expected FWM signal of the non-equilibrium e-h plasma have been treated recently by Vu *et al.*[8] using bare Coulomb potential for times shorter than the build-up time of screening. While the density-dependence of the optical spectra of a quasi-equilibrium 2D magneto-plasma have been calculated,[9] the kinetics of a magneto-plasma has been studied neither experimentally nor theoretically. Moreover, the existing theory for the kinetics with a magnetic field is also not yet developed as far as in the field-free case. However, as experimental studies of the relaxation and dephasing kinetics in QW's and superlattices are in progress[10], we will provide a first calculation of the femtosecond FWM signal of a resonantly excited magneto-plasma in a single quantum well. We concentrate on the study of carrier-carrier scattering, while phonon and disorder scattering is not considered.

A strong magnetic field perpendicular to the QW plane forces the carriers on cyclotron orbits, thus causing an additional quantum confinement. In a magnetic field of the order of more than 10T only a few Landau levels both in the conduction and valence band have to be considered. The high degeneracy of these Landau levels is partially lifted by spatial inhomogeneities and by size effects. The numerical treatment of the broadening due to disorder, e.g. interface fluctuations, would require a stochastic averaging over many FWM signal calculations which is beyond present day numerical possibilities for the complex carrier kinetics treated here. Therefore, we lift the degeneracy partially by a weak parabolic confinement potential. The Landau levels are broadened by this confinement into Landau subbands with a band width of about 2 meV. This weak parabolic confinement allows to treat the single-particle Schrödinger equation still exactly in the presence of the magnetic field.[11] These eigenfunctions of the 2D electron provide a convenient expansion basis for the non-equilibrium many-body problem. A strong quantum confinement — here caused by the QW and the strong magnetic field — is generally believed to slow down the relaxation kinetics because of the reduction of the phase space for scattering processes.[12] Indeed, for low-density magneto-excitons an increase in dephasing time has been observed.[13] However, this rule does not apply to Coulomb scattering, as has been shown recently for the example of exciton-exciton scattering in QW wires.[14] For decreasing wire width a reduction of the dephasing time has been found and explained in terms of the increase of the Coulombic interaction matrix elements which overcompensated the reduction of phase space for the scattering processes. Therefore it is not obvious, how the Coulomb intra- and inter-Landau-subband scattering will influence the resulting dephasing time in a dense magneto-plasma in detail.

We present a kinetic study for a femtosecond laser-pulse excited 2D dense non-equilibrium magneto-plasma in a QW in the framework of the semiconductor Bloch equations combined with Coulomb scattering rates (Sec. II). We expand the density matrix of a two-band semiconductor in the eigenfunctions of the 2D electron in the presence of the strong magnetic field and the weak parabolic confinement. We formulate the scattering terms for the population distribution functions of the various Landau subbands and for the optically induced polarization components between the Landau-subbands in the conduction and valence band in the form of non-Markovian quantum kinetic scattering integrals[3] and in the form of semiclassical Boltzmann-type scattering rates. Pronounced quantum kinetic effects are expected for time scales shorter than typical inverse frequencies. For the considered high magnetic fields, the cyclotron frequencies are so large that quantum kinetic effects should be of minor importance. Furthermore, we prefer the use of the simpler semiclassical kinetics, because there exist still some conceptual difficulties for the quantum kinetic description, connected with the spectral electron Green functions in a strong magnetic field, as will be discussed below. We calculate the time-resolved (TR) and time-integrated (TI) four-wave mixing (FWM) signals for two 50 fs pulses by taking into account up to three Landau subbands in both the valance band and the conduction band. The carrier frequency of the two delayed pulses is tuned slightly above the un-renormalized energy gap. We simplify the problem by assuming equal effective electron and hole masses, as it can be approximately realized in strained QW's. Naturally, unequally effective masses will lead to more complicated quantum beat structures in the FWM signals and modify to some extend also the resulting relaxation and dephasing rates. Thus our present study should be seen only as a first idealized model calculation. The detailed numerical results based on the semiconductor Bloch equations with Boltzmann-type scattering kinetics are presented in Sec. III for intermediate and high plasma densities. The FWM signal is calculated by an adiabatic projection technique which is appropriate for thin samples where propagation effects are not important. For many conditions pronounced quantum beat structures with two times the cyclotron frequency are obtained both in the TR and TI FWM signals. Furthermore, often relaxation oscillations are seen between the populations of two subbands, before they relax to their stationary values. The dephasing times obtained from the TI FWM signal are surprisingly short and strongly modulated as a function of the magnetic field. The unexpectedly short resulting dephasing times between 100 and 200 fs depend not only on the field values, but also on the detuning, the pulse width and the excited carrier densities. In spite of the remaining conceptual difficulties we present also first quantum kinetic calculations and compare the FWM signals with those obtained with Boltzmann-type kinetics in Sec. IV. A conclusion of our main results is given in Sec. V. In an appendix we give a list of the analytically calculated Coulomb matrix elements for the first three subbands.

II. MODEL AND KINETIC EQUATIONS

A. Model and Hamiltonian

We start our investigation of a quantum well in the x-y plane which is further restricted by an additional weak lateral confinement in x direction which lifts the degeneracy of the Landau levels partially and provides a weak inhomogeneous broadening. The confinement is assumed to be given by a harmonic oscillator potential for the lower-lying states. This model has been used with a strong additional confinement for the theory of the optical properties of thermal magneto-plasmas in QW wires.[11] A strong magnetic field $B \geq 10$T is applied perpendicular to the well. We assume electron-hole symmetry, *i.e.* $m_e = m_h \equiv m$ with m_e (m_h) denoting the effective electron (hole)mass. Within the Landau gauge $\mathbf{A} = xB\mathbf{e}_y$ and effective mass approximation[15] to the lowest QW subband, the stationary 2D Schrödinger equation of a single electron can be solved exactly ($\hbar = c = 1$):

$$\left[\frac{1}{2m}\left(-\frac{\partial^2}{\partial x^2} + (\frac{1}{i}\frac{\partial}{\partial y} - exB)^2\right) + \frac{1}{2}m\Omega x^2 - E_{cnk}\right]\psi_{nk}(x,y) = 0 \ , \qquad (1)$$

with the shifted Landau eigenfunction

$$\psi_{nk}(x,y) = \frac{e^{iky}}{\sqrt{L_y}}\phi_n(x - \delta x_k), \qquad (2)$$

where $\phi_n(x)$ is the eigenfunction of n-th Landau level ($n = 0,\, 1,\, \cdots$) and reads[15]

$$\phi_n(x) = \left(\frac{\alpha}{\sqrt{\pi}2^n n!}\right)^{1/2} H_n(\alpha x)e^{-\frac{1}{2}\alpha^2 x^2} \ , \qquad (3)$$

with $H_n(x)$ standing for the n-th order Hermite polynomial and $\alpha = \sqrt{m\Omega_x}$ is the inverse of the amplitude of the zero-point fluctuations. Ω_x is the effective oscillation frequency $\Omega_x = \sqrt{\Omega^2 + \omega_c^2}$, where $\omega_c = eB/m$ is the cyclotron frequency and Ω is the frequency of the additional confinement potential. The shift $\delta x_k = -\omega_c k/(m\Omega_x^2)$ results from the balance between the Lorentz force and the harmonic restoring force $e(k/m)B = m\Omega_x^2 \delta x_k$.

The single-particle energy spectrum of a conduction band electron in n-th Landau level and with momentum k is given by $E_{cnk} = E_g/2 + \varepsilon_{nk}$ with

$$\varepsilon_{nk} = \frac{\Omega^2}{\Omega_x^2}\frac{k^2}{2m} + \Omega_x(n + \frac{1}{2}) \tag{4}$$

and E_g standing for the energy gap. The dependence of the energy on the momentum in y-direction results from the additional confinement of the QW, which broadens each Landau level into a small Landau subband. The momenta are restricted to

$$|k| \leq L_x m\Omega_x^2/(2\omega_c) \tag{5}$$

because the center of cyclotron should lie within the sample width L_x.[15] It is interesting to notice that when $\omega_c \gg \Omega$, the inhomogeneous broadening is of the same for all magnetic fields as the increase of k space in Eq. (5) is totally compensated by the increase of the effective mass in Eq. (4).

With Coulomb interaction and with the interaction with a coherent classical light field, the many-body Hamiltonian for the electrons in the conduction and valence bands is in the basis of above given magnetic eigenfunctions

$$\begin{aligned} H = \sum_{\nu nk} E_{\nu nk} c^\dagger_{ink} c_{ink} + \frac{1}{2} \sum_{\nu_1\nu_2;nmij;kk'q} V_{ni;jm}(q,k,k') \\ \times c^\dagger_{\nu_1 nk+q} c^\dagger_{\nu_2 ik'-q} c_{\nu_2 jk'} c_{\nu_1 mk} + H_I \ , \end{aligned} \tag{6}$$

with $\nu = c$ and v standing for the conduction band and the valence band respectively. $E_{vnk} = -E_{cnk}$ is the energy spectrum of an electron in the valence band.

The Coulomb interaction matrix elements $V_{ni;jm}(q,k,k')$ describes the scattering of an electron with momentum k from m-th Landau subband to n-th subband with momentum $k+q$ and an electron with momentum k' from j-th subband to i-th with momentum $k'-q$. Due to the assumed e-h symmetry, these four Landau subbands can be either in the conduction band or in the valence band. The matrix elements are given in terms of the shifted magnetic eigenfunctions by the following integral

$$\begin{aligned} V_{ni;jm}(q,k,k') = \sum_{q_x} \frac{2\pi e^2}{\epsilon_0\sqrt{q^2+q_x^2}} \int dx dx' e^{-iq_x(x-x')} \\ \times \phi_n^*(x - \delta x_k + \delta x_q)\phi_i^*(x' - \delta x_{k'} - \delta x_q)\phi_j(x' - \delta x_{k'}) \\ \times \phi_m(x - \delta x_k) \ , \end{aligned} \tag{7}$$

ϵ_0 is the background dielectric constant. After substituting $x \longrightarrow x + \delta x_k$ and $x' \longrightarrow x' + \delta x_{k'}$ in Eq. (7), one gets

$$\begin{aligned} V_{ni;jm}(q,k,k') = \sum_{q_x} \frac{2\pi e^2/\epsilon_0}{\sqrt{q^2+q_x^2}} \int dx dx' \exp\{-iq_x[x - x' \\ + \lambda(k-k')]\}\phi_n^*(x+\delta x_q)\phi_i^*(x'-\delta x_q)\phi_j(x')\phi_m(x) \ , \end{aligned} \tag{8}$$

with $\lambda = -m\omega_c/\alpha^2$. After an approximation concerning the momentum dependence, the integrals of Eq. (8) may be carried out analytically. In the appendix the corresponding approximation and the final expressions of $V_{ni;jm}(q,k,k')$ in terms of zeroth- and first-order modified Bessel functions are given.

H_I in Eq. (6) denotes the dipole coupling with the light field $E(t)$. In the assumed e-h symmetry it contains only transitions between Landau subbands of the same order:

$$H_I = -d \sum_{nk} E(t)(c^\dagger_{cnk} c_{vnk} + h.c.) \ . \tag{9}$$

In this equation, d denotes the optical-dipole matrix element. The light field is further split into $E(t) = E_0(t)e^{i\omega t}$ with ω being the central frequency of the coherent pulse. $E_0(t)$ describes a Gaussian pulse $E_0 e^{-t^2/\delta t^2}$ with δt denoting the pulse width.

B. Kinetic Equations

Following the same scheme as for the magnetic-field-free case in Ref. 3, appropriately modified, one may build the semiconductor Bloch equations for the QW in a strong perpendicular magnetic field B in the basis of the magnetic eigenfunctions as follows:

$$\dot\rho_{\nu,n,\nu',n',k} = \dot\rho_{\nu,n,\nu',n',k}|_{\rm coh} + \dot\rho_{\nu,n,\nu',n',k}|_{\rm scatt} \ . \tag{10}$$

Here $\rho_{\nu,n,\nu',n',k}$ represents the single-particle density matrix. The diagonal elements describe the carrier distribution functions $\rho_{\nu,n,\nu,n,k} = f_{\nu nk}$ of the n-th Landau subband and the wavevector k as diagonal elements, and the off-diagonal elements describe the interband polarization components, e.g. $\rho_{c,n,v,n,k} = P_{nk}e^{-i\omega t}$. For the assumed e-h symmetry, $f_{enk} \equiv f_{hnk} \equiv f_{nk}$ and the polarization has only components between subbands of the same quantum number n in the conduction and valence band, which simplifies the problem considerably.

The coherent part of the equation of motion for the distribution function is in the rotating wave approximation given by

$$\begin{aligned} \dot f_{nk}\Big|_{\rm coh} = -2{\rm Im}\{[dE_0(t)/2 + \sum_{m,q} V_{nm;nm}(q,k,k) \\ \times P_{mk+q}(t)]P^*_{nk}(t)\} \ . \end{aligned} \tag{11}$$

The first term describes the generation rate by the laser pulse. d is the optical dipole matrix element. For the assumed e-h symmetry transitions between different subband quantum numbers are not allowed. The second term describes the exchange interaction correction of the exciting laser by the e-h attraction, thus it can be seen as a local field correction of the time-dependent bare Rabi frequency $dE_0(t)$. The retarded quantum kinetic scattering rates for the considered bare Coulomb potential scattering are given by[3,8]

$$
\begin{aligned}
\dot{f}_{nk}\Big|_{\mathrm{scatt}} &= -8 \sum_{qk'mij} |V_{ni;jm}(q,k,k'+q)|^2 \\
&\times \int_{-\infty}^{t} dt' \mathrm{Re}\{ e^{[-i(\varepsilon_{mk-q}-\varepsilon_{nk}+\varepsilon_{jk'+q}-\varepsilon_{ik'})-\Gamma](t-t')} \\
&\times [f_{nk}(t')f_{ik'}(t')(1-f_{mk-q}(t'))(1-f_{jk'+q}(t')) \\
&- f_{mk-q}(t')f_{jk'+q}(t')(1-f_{nk}(t'))(1-f_{ik'}(t')) \\
&- P^*_{nk}(t')P_{mk-q}(t')(f_{ik'}(t')-f_{jk'+q}(t')) \\
&- P_{jk'+q}(t')P^*_{ik'}(t')(f_{nk}(t')-f_{mk-q}(t'))]\} \ . \qquad (12)
\end{aligned}
$$

In the derivation of this formula vertex corrections have been neglected. The scattering self-energy is evaluated in time-dependent RPA. Successively, the Coulomb potential is taken as a bare instantaneous potential and the two-time-dependent particle propagators have been expressed in terms of single-time density matrix elements and retarded (or advanced) Green functions using the generalized Kadanoff-Baym ansatz. For simplicity the retarded (and advanced) Green functions have been approximated by a diagonal free-particle Wigner-Weiskopf form, i.e. $G^r_{nk}(t,t') = G^{a*}_{nk}(t',t) = -i\Theta(t-t')e^{[-i(E_g/2+\varepsilon_{nk})-\gamma](t-t')}$. The effective damping Γ in Eq. (12) is the sum of the four imaginary parts of the retarded electron self-energy which is assumed to be simply the damping constant γ, so that $\Gamma \simeq 4\gamma$. We will discuss later that this approximation for the imaginary part of the retarded e-self-energy leads to some unphysical features in the quantum kinetics of the considered magneto-plasma. For further progress in the quantum kinetics of a magneto-plasma, the calculations of the spectral functions have to be made more self-consistent in order to include the retarded onset and the magnetic field dependence of damping and the band mixing by the coherent light pulses and the mean-field Coulomb interactions. These refinements have been developed already for the simpler case of scattering with optical phonons without magnetic field.[3,16,19] However, for the time being the complexity of the Coulomb quantum kinetics in a magneto-plasma prevents us to include these improvements in the present numerical evaluation.

The coherent time evolution of the interband polarization components are

$$
\begin{aligned}
\dot{P}_{nk}\Big|_{\mathrm{coh}} &= -i\delta_n(k)P_{nk}(t) + i\Big[dE_0(t)/2 \\
&+ \sum_{m,q} V_{nm;nm}(q,k,k)P_{mk+q}(t)\Big][1-2f_{nk}(t)] \ . \qquad (13)
\end{aligned}
$$

The first term gives the free evolution of the polarization components with the detuning

$$
\delta_n(k) = 2\varepsilon_n(k) - \Delta_0 - 2\sum_{m,q} V_{nm;nm}(q,k,k)f_{mq}(t) \quad (14)
$$

with $\Delta_0 = \omega - E_g$. Δ_0 is the detuning of the center frequency of the light pulses with respect to the unrenormalized band gap. The second term in Eq. (13 describes again the excitonic correlations in the magneto-plasma, while the final factor describes the Pauli blocking.

The dephasing of the polarization components are determined by the following quantum kinetic scattering integral

$$
\begin{aligned}
\dot{P}_{nk}\Big|_{\mathrm{scatt}} &= -4 \sum_{qk',mij} |V_{ni;jm}(q,k,k'+q)|^2 \\
&\times \int_{-\infty}^{t} dt' \Big\{ \Big[e^{[-i(\varepsilon_{mk-q}+\varepsilon_{nk}+\varepsilon_{jk'+q}-\varepsilon_{ik'}-\Delta_0)-\Gamma](t-t')} \\
&\times (P_{nk}(t')N_{mji}(k-q,k',q,t') - P_{mk-q}(t') \\
&\qquad \times N_{nji}(k,k',q,t'))\Big] - \Big[n \leftrightarrow m; \\
&i \leftrightarrow j; k \leftrightarrow k-q; k' \leftrightarrow k'+q\Big]\Big\} - \frac{P_{nk}(t)}{T_2} \ , \qquad (15)
\end{aligned}
$$

with the population factor

$$
\begin{aligned}
N_{nji}(k,k',q,t') &= (1-f_{nk}(t'))(1-f_{jk'+q}(t'))f_{ik'} \\
&+ f_{nk}(t')(1-f_{ik'}(t'))f_{jk'+q}(t') - P_{jk'+q}(t')P^*_{ik'}(t') \ , \quad (16)
\end{aligned}
$$

and the energy difference $\delta_n(k) = 2\varepsilon_n(k) - \Delta_0 - 2\sum_{m,q} V_{nm;nm}(q,k,k)f_{mq}(t)$. $\Delta_0 = \omega - E_g$ is the detuning with respect to the unrenormalized band gap. Here T_2 is introduced phenomenologically to describe additional slower scattering processes. Eqs. (10)-(12), (13) and (15) are the quantum kinetic Bloch equations for a magneto-plasma.

In the longtime limit the quantum kinetic scattering integrals be transformed into Markovian Boltzmann-type scattering rates by pulling the slowly varying distributions and polarization components outside the scattering integrals at the upper limit t and by replacing the memory kernels $\int_{-\infty}^{t} dt' \exp\{[-i(\varepsilon_{mk-q} - \varepsilon_{nk} + \varepsilon_{jk'+q} - \varepsilon_{ik'}) - \Gamma](t-t')\}$ in Eq. (12) by $2\pi\delta(\varepsilon_{mk-q} - \varepsilon_{nk} + \varepsilon_{jk'+q} - \varepsilon_{ik'})$ and $\int_{-\infty}^{t} dt' \exp\{[-i(\varepsilon_{mk-q} + \varepsilon_{nk} + \varepsilon_{jk'+q} - \varepsilon_{ik'} - \Delta_0) - \Gamma](t-t')\}$ in Eq. (15) by $2\pi\delta(\varepsilon_{mk-q} + \varepsilon_{nk} + \varepsilon_{jk'+q} - \varepsilon_{ik'} - \Delta_0)$ in the limit of vanishing damping. In our calculations we use for numerical convenience energy resonances with a small Gaussian damping, which does not lead to such severe violations of the energy conservation as the Lorentzian resonances do.

It is noted that besides the e-h symmetry, we have further assumed that Coulomb Auger scattering across the gap can be neglected.

III. NUMERICAL RESULTS BASED ON BOLTZMANN KINETICS

We perform a numerical study of the Bloch equations in the Boltzmann limit to study TR and TI FWM signals for high magnetic fields ($B > 10$ T) for two degenerate Gaussian pulses of a width of 50 fs and a variable delay time τ. The pulses travel in the direction $\mathbf{k}_1$ and $\mathbf{k}_2$. We use an adiabatic projection technique in order to calculate the polarization in the FWM direction with wavevector $2\mathbf{k}_2 - \mathbf{k}_1$ described in detail in Ref. 16. This technique is suitable for optically thin crystals, where the spatial dependence can be treated adiabatically.[17] To do so, we replace the single-pulse envelope function in Eq. (11) by two delayed pulses $E_0(t) = E_0(t) + E_0(t-\tau)e^{i\varphi}$ with the relative phase $\varphi = (\mathbf{k}_2 - \mathbf{k}_1)\cdot\mathbf{x}$ resulting from the different propagation directions. The projection technique is used with respect to this phase. We further assume a resonant excitation with a fixed excess energy of $\Delta_0 = 26.4$ meV. The intensity of each pulse will be given by $\int_{-\infty}^{\infty} dE_0(t)dt = \chi\pi$, where χ denotes the fraction of a π-pulse defined without local field corrections. Except m_h which is assumed to be equal to m_e, all the other material parameters are taken for bulk GaAs with an exciton Rydberg of 4.2 meV and a Bohr radius of 14 nm. For the sake of weak confinement, the harmonic oscillator frequency Ω is assumed to be $0.1\omega_c$ for $B = 7$ T, corresponding to $\Omega = 1.2$ meV. By fitting the energy Ω with the energy splitting to the two lowest subbands of a rectangular square well $3\pi^2/(2mL_x^2)$, we get the width in the additional confinement direction to be $L_x = 118$ nm.[11]

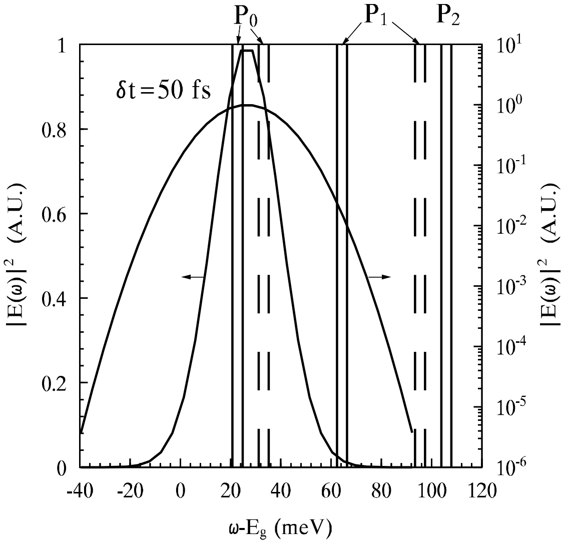

FIG. 1. The pulse intensity spectrum $|E(\omega)|^2$ plotted in both linear and log scale for a 50 fs pulse, together with the unrenormalized energybands for the optical transitions between Landau subbands n(=0, 1, 2) plotted as solid lines for $B = 12$ T and as dashed lines for $B = 18$ T.

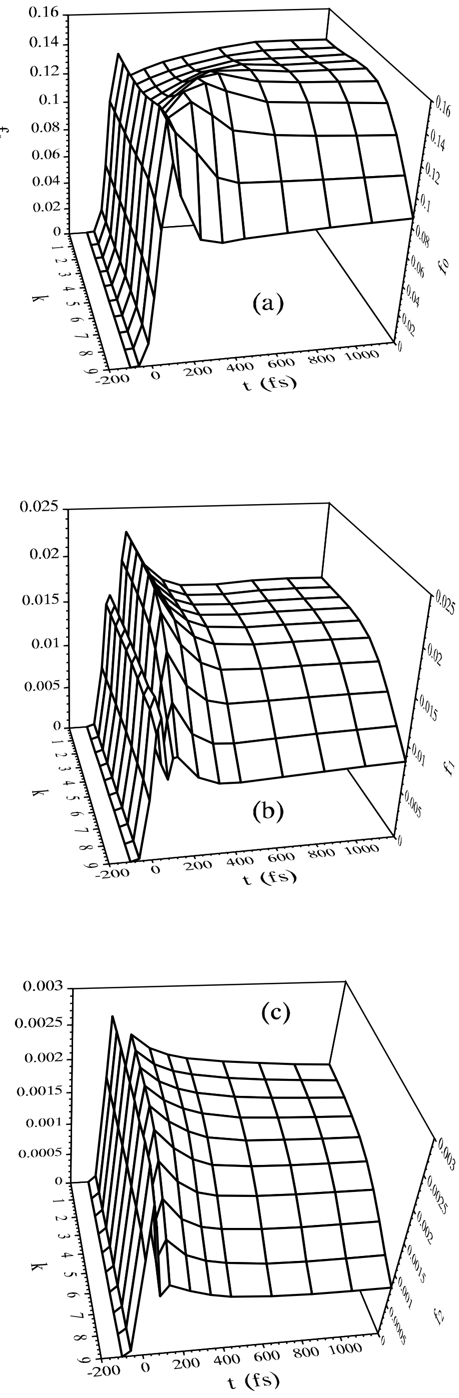

FIG. 2. The distribution functions of three Landau subbands f_0, f_1 and f_2 are plotted as functions of t and k for a one-pulse excitation with $B = 12$ T. The units of k in the figures are one tenth of the maximum allowed value of k defined in Eq. (5).

In Fig. 1 we plot the pulse spectrum together with the three transitions bands for two magnetic fields of $B = 12$ T (solid lines) and 18 T (dashed lines). The first transition band corresponding to P_0 is due to transitions between the lowest Landau subband $n = 0$ in the valance band to the lowest subband $n = 0$ in the conduction band. This transition band starts an effective frequency Ω_x above the band gap at least in the low-density limit. Similarly the second transition band for the n=1 Landau subbands in both valence and conduction bands requires the excess energy $3\Omega_x$. The Hartree-Fock terms in Eq. (14) may red-shift the energy of transition for the initial stage of excitation. From Fig. 1 we see that for high magnetic fields, the pulse mainly populates in the lowest Landau subband.

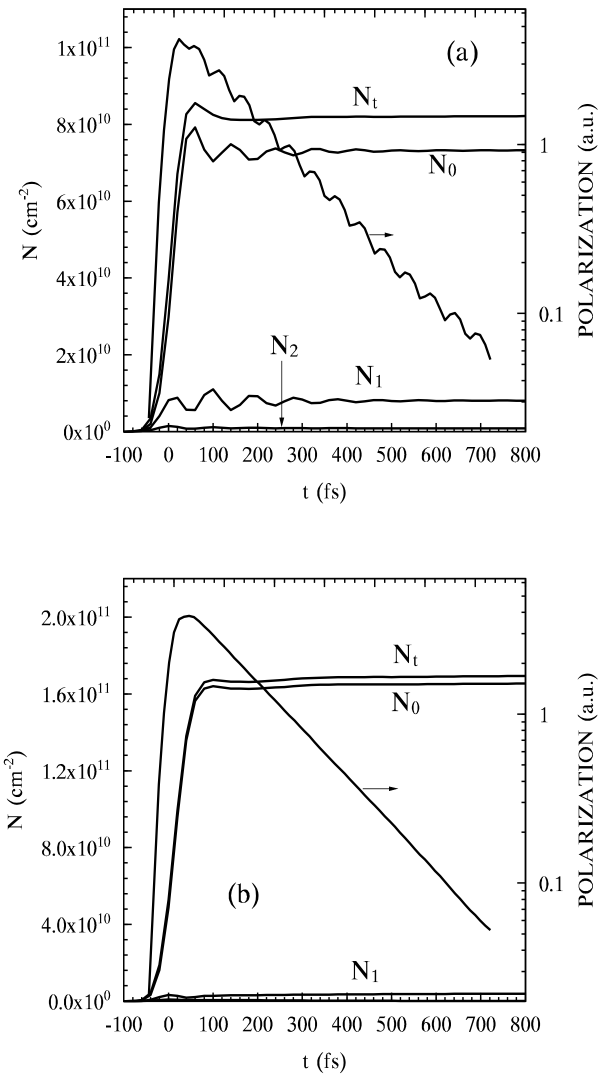

FIG. 3. Electron densities of three Landau subbands N_i and the total density N_t and the incoherently summed polarization plotted against time t for $B = 12$ T (Fig. 3(a)) and 18 T (Fig. 3(b)).

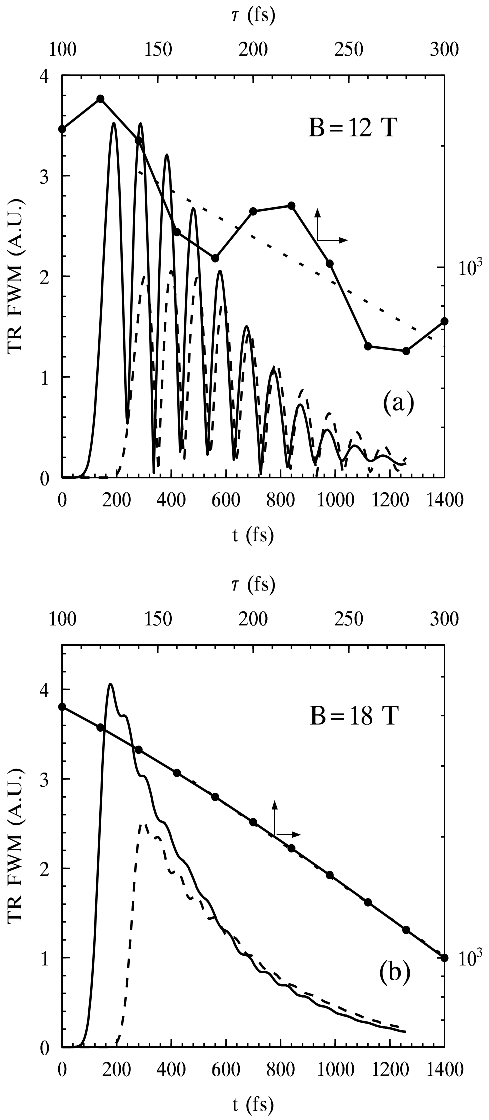

FIG. 4. TR and TI FWM signals versus time t and delay τ, respectively, for $B = 12$ T (Fig. 4(a)) and 18 T (Fig. 4(b)). For TR FWM, the solid curve is for $\tau = 120$ fs and dashed curve for 240 fs. The dotted line is the exponential fit to the TI FWM signal. Note that the scale of the delay time τ for TI FWM signals (top frame) is different from the time scale of the TR FWM signals (bottom frame).

As mentioned before, we include in our calculations three Landau subbands in the valence and conduction band. It is important to include higher Landau subbands for the kinetics after the excitation. In principle it is true even in situations where the pulses mainly excite e's and h's only in the pair of the lowest Landau n=0 subbands: A certain number of e's excited in the n=1 Landau subband can only relax to the n=0 subband, if simultaneously the same number of e's is excited from the n=1 to the n=2 subband if only three subbands are included. On the other hand, say if one includes up to 5 Landau subbands, then it is possible to only scatter one electron from the second Landau subband to the fifth subband and in the mean time to release three electrons from the second subband to the lowest subband. Therefore, a too small number of Landau subbands may change the Coulomb kinetics. For this reason, we restrict ourselves to the high magnetic field regime in which for the chosen detuning e's and h's are excited mainly in the lowest n=0 Landau subbands. More Landau subbands are necessary in order to extend the kinetics to lower magnetic fields or for larger detunings. However, the expansion of number of matrix elements $V_{ni;jm}$ increases as N^4 with N being total number of Landau subbands considered. With $N = 3$ in our model, the number of form factors is already 81, while it will be 256 with $N = 4$.

A. Intermediate-density case

We first discuss the Boltzmann kinetics for an intermediate excitation density. To do so, we choose a pulse with $\chi = 0.1$. We first show the distribution functions $f_{nk}(t)$ for $n = 0$, 1 and 2 versus t and k for a one-pulse excitation in Fig. 2 for $B = 12$ T. Here and hereafter, the additional transverse relaxation time T_2 is taken as 300 fs. The energy conserving δ-functions in the collision terms are replaced by Gaussian functions with a width $\sigma = 0.66$ meV which is much smaller than both ω_c and the inhomogeneous broadening. Note again that k is limited by Eq. (5). One sees how the carriers relax at later times in the lower k-states of the Landau subbands. We plot the various carrier densities $N_i(t) = \sum_k f_{ik}(t)$ against time t for the magnetic fields $B = 12$ T (Fig. 3(a)) and 18 T (Fig. 3(b)). For $B = 12$ T, one sees pronounced relaxation oscillations of the populations of the lowest subbands $N_0(t)$ and $N_1(t)$ in the first 400 fs. The period of these relaxation oscillations (≈ 60 fs) with successive overshoots in the population of the Landau subband $n = 0$ and $n = 1$ is given by the characteristic interband Coulomb scattering rate between these two lowest subbands. The total carrier density $N_t = \sum_i N_i$ shows a slight Rabi flopping overshoot. The incoherently summed polarizations $P(t) = \sum_{ik} |P_{ik}|$ for the two fields are also plotted in the same figures. Strong quantum beats with frequency $2\omega_c$ are revealed in the polarization for lower magnetic fields up to 16 T. This effect may be measured by FWM. For $B > 16$ T, both the population oscillation and the beating of the polarization amplitude die out (see Fig. 3(b)). Moreover, one sees that in the latter case the carriers are excited practically only in the lowest Landau subband.

In Fig. 4 we plot typical TR FWM signals versus time t for $B = 12$ T (Fig. 4(a)) and 18 T (Fig. 4(b)) for two pulses with the delay times $\tau = 120$ fs (solid curve) and 240 fs (dashed curve), respectively. We find strong beating for lower magnetic fields, whereas for higher fields the beating becomes weaker. Only very small beats are found for $B = 18$ T in Fig. 4(b). The beating totally disappears for $B = 20$ T. The beating frequency for the TR FWM signal is exactly $2\omega_c$ for all magnetic fields where beating exists. From the TI FWM signal as a function of the delay time τ one can obtain the effective dephasing time. Therefore we plot the TI FWM signals in the same figures, however, projected on the right and top scales. Again one observes quantum beats in the TI FWM signals for lower fields. Similar beating effect has been obtained based on a three-level model in explaining heavy hole-light hole beats by Leo *et al.*.[18] Moreover, the beats become weaker when the magnetic field increases because then the second subband becomes less important. For $B = 16$ T the beating has already disappeared in TI FWM which means that the polarization components P_{1k} are negligible in comparison to P_{0k} . This is consistent with Fig. 3(b), where the electron (hole) population in the second Landau subband is extremely low and the beating structure disappears in the incoherently summed polarization. The beating frequency for the lower field is also $2\omega_c$. Note again the different scales used for t and τ. The dotted lines in both figures are the exponential fits to the TI FWM signal. From the fit one gets the effective dephasing time which is plotted as a function of the magnetic field B in Fig. 5. Interestingly, we find for large magnetic fields that the dephasing time decreases with increasing field for 10 T$< B < 16$ T. However, there is a transition at 16 T. For $B > 16$ T the dephasing time increases with increasing field, although much slower than it decreased before.

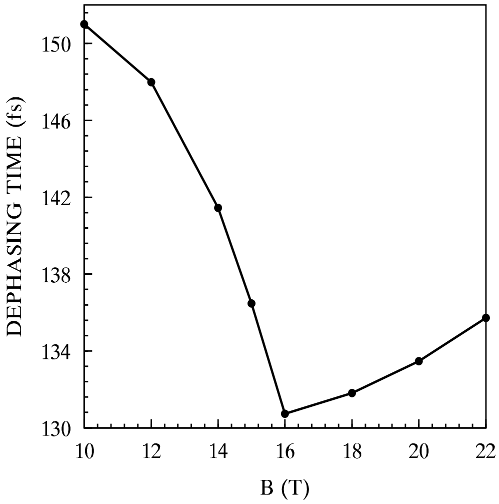

FIG. 5. Dephasing time as a function of B.

For a fixed pulse, several effects compete with each other when the magnetic field increases. On one hand, the number of Landau subbands which contribute to the Coulomb scattering kinetics decreases. In particular the contributions to the dephasing from the intra- and inter-subband scattering of the higher Landau subbands as well as the inter-subband scattering between the higher and lower subbands decrease. For large populations in one subband the Pauli blocking may further reduce also the intra-band scattering rates. All these effects increase the dephasing time. On the other hand, with increasing B field the degeneracy of Landau subbands increases and the matrix elements of the Coulomb scattering of Eq. (8) become larger. How an increasing degeneracy increases the scattering rates can be seen from Eqs. (12) and (15) in the extreme limit where the confinement is lifted. Then there is no k and k' dependence in either distribution functions or polarization functions. Therefore $\sum_{k'}$ is replaced by $Sm\omega_c/(2\pi)$ (S standing for the 2D area)[15] which increases as B increases. Such an ef-

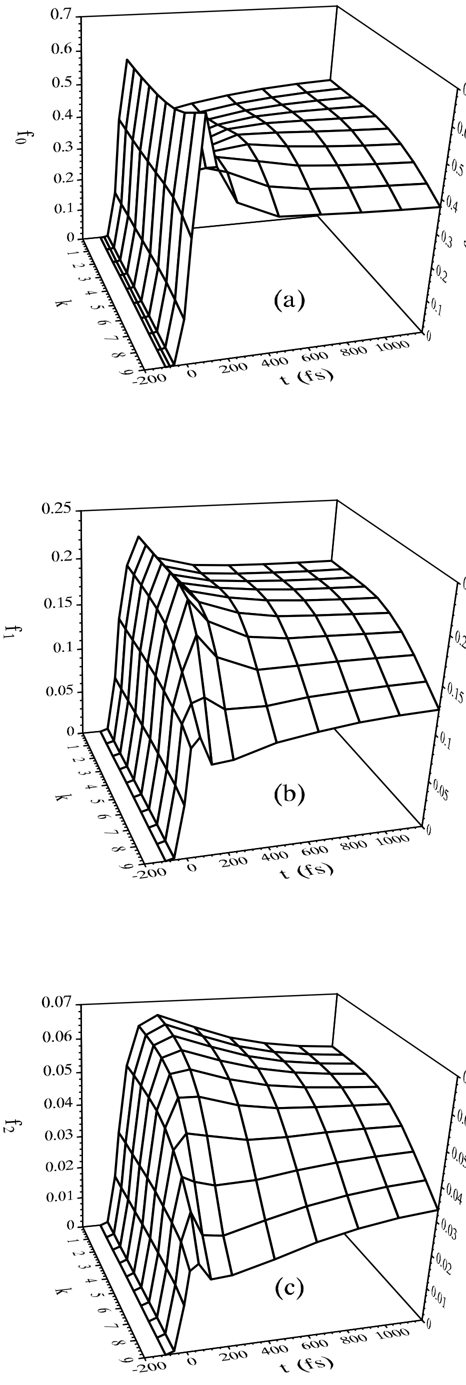

FIG. 6. Distribution functions of three Landau subbands f_0, f_1 and f_2 versus t and k for one-pulse excitation for $B = 12$ T. The units of k in these figures are one tenth of the maximum allowed value of k defined in Eq. (5).

fect is also kept after the weak broadening in k space is included. Thus both the increased degeneracy and the increased Coulomb matrix elements reduce the dephasing time. Particularly, for $B \geq 16$T the above discussed increase in the scattering rates is overcompensated by the loss of the contributions of the inter-subband scattering processes and the reduction of the intra subband scattering due to Pauli blocking, so that a net slow increase of the dephasing time with increasing B field is obtained. For 10T $\leq B \leq$ 16T the increasing degeneracy and the increasing Coulomb matrix elements dominate over the reduction of inter-subband scattering so that the dephasing time decreases with increasing B field.

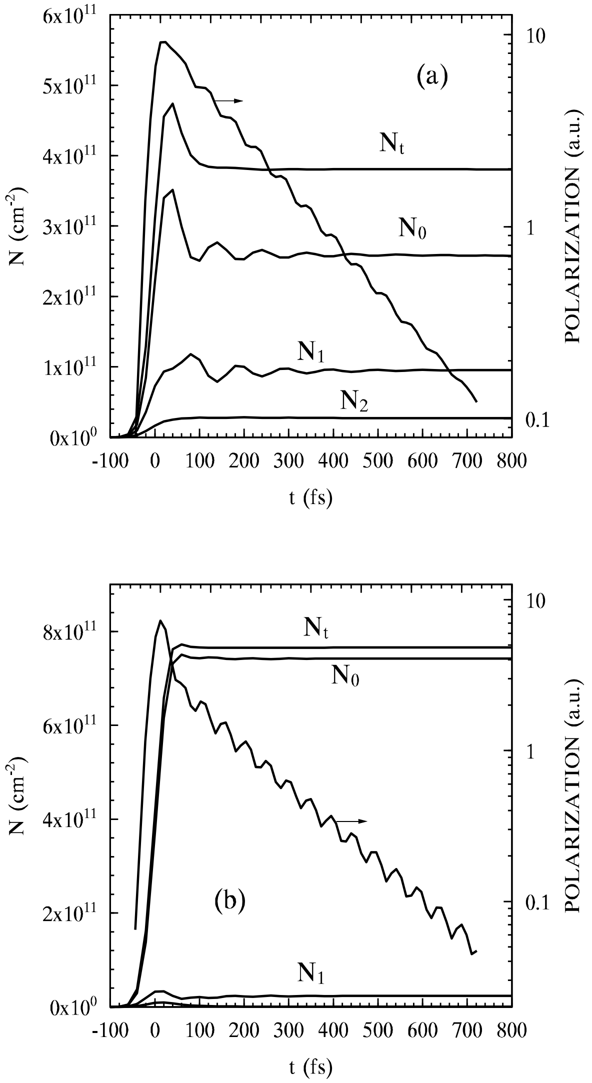

FIG. 7. Electron density and incoherently summed polarization are plotted against time t for $B = 12$ T (Fig. 3(a)) and 18 T (Fig. 3(b)). N_n ($n = 0$, 1, and 2) is carrier density in n-th Landau subband. $N_t = N_1 + N_2 + N_3$ is the total density.

B. High-density case

In order to obtain a dense magneto-plasma with strong carrier interaction, we choose $\chi = 0.3$ corresponding roughly to a $\pi/3$ pulse, which provides a very high excitation density. The detuning is kept to be $\Delta_0 = 26.4$ meV. Note that the local field renormalization will actually turn the optical Bloch vector through an angle considerably larger than $\pi/3$. We show the distribution function $f_{nk}(t)$ with $n = 0$, 1 and 2 versus t and k for one-pulse excitation in Fig. 6 for $B = 12$ T.

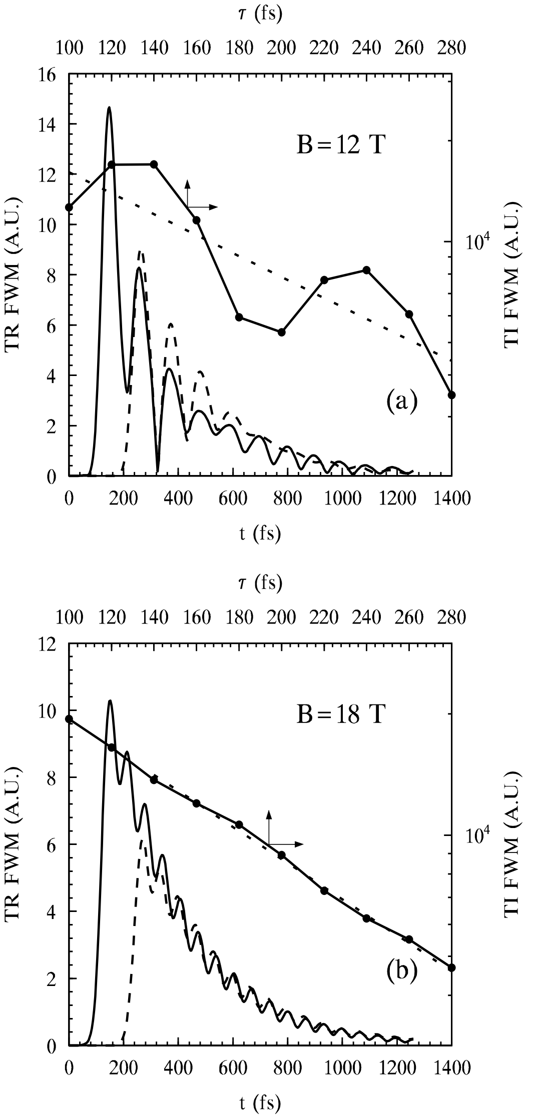

FIG. 8. TR and TI FWM signals versus time t and delay τ respectively for $B = 12$ T (Fig. 4(a)) and 18 T (Fig. 4(b)). For TR FWM, the solid curve is for $\tau = 120$ fs and dashed curve for 240 fs. The dotted line along TI FWM signal is the exponential fit to the TI FWM signal.

From the figure one can see that the carrier distribution function for the lowest Landau subband is close to 0.5. This number approaches 1 when B is around 18 T. One sees a pronounced Rabi-flopping in the two lowest Landau subbands. We further plot the carrier density against time t for two different magnetic fields $B = 12$ T (Fig. 7(a)) and 18 T (Fig. 7(b)). The incoherently summed polarizations for the two fields are also plotted in the same figures. Differing from the intermediate-density case, strong quantum beats are revealed for both field strengths, while the population relaxation oscillations with a period of about 100 fs are again only well resolved for the low-magnetic field case ($B = 12$ T). Again, the lowest Landau subband is always excited most strongly.

In Fig. 8 we plot again typical TR FWM signals against time t for $B = 12$ T (Fig. 4(a)) and 18 T (Fig. 4(b)) for two pulses with the delay times $\tau = 120$ fs (solid curve) and 240 fs (dashed curve), respectively. Similar to the intermediate-density case, we find quantum beating for fields as high as 20 T with a frequency of exactly $2\omega_c$, although for large fields the beating become weaker. The TI FWM signals are plotted in the same figures as functions of delay time τ (upper time scale). Again one observes quantum beats in the TI FWM signals. Interestingly, the beating frequency is close to that in the incoherently summed polarization and is a little bit smaller than $2\omega_c$ for higher fields. For example, when $B = 18$ T, $\pi/\omega_c = 66.5$ fs whereas from the beating in TI FWM, one finds a period around 76 fs. This difference may be understood in terms of many-body effects, such as band gap renormalization, Pauli blocking and excitonic enhancement. We conclude that the quantum beats in the high-density case are also caused by interferences between the optically induced polarizations $P_{n=0k}$ and $P_{n=1,k}$ of the two lowest subbands.

The effective dephasing is plotted as a function of the magnetic field B in Fig. 9. Once more we find a gradual overall decrease of the dephasing time with increasing field in the regime from 10 to 20 T. This is in agreement with our earlier results in the intermediate-density case for 10 T$< B <$ 16 T. The dephasing is mainly controlled in the whole range by the kinetics in the lowest two Landau subbands. Compared to the intermediate-density regime, one observes a sharp dip around 15 T in the dephasing time. By investigating the distribution function, we find the dip around 15 T is mainly due to the function of the second pulse. When B is smaller than 15 T, the second pulse further pumps electrons from valence band to conduction band. Due to the density dependent red shift of the subbands and the Pauli blocking for the optical transition in the lowest subband, the second pulse increases the population of the second subband relative to that of the first one. The ratio of the densities in the lowest two subbands N_0/N_1 falls from around 5.7 after the first pulse to 4 after the second pulse when B=14 T, and that number goes from 8 to 3.9 for $B = 15$ T. This means the role of second subband becomes more important to the dephasing. This gives rise to the sharp decrease of the dephasing time. However for $B > 15$ T, the lowest Landau subband is already highly populated and due to the high magnetic field value, the second Landau subband is already relatively far away from the center of the pulse, so that the second pulse depopulates the electrons from the first conduction subband. Although this makes again the density of lowest subband closer to the second one, the ratio N_0/N_1 after the second pulse goes from 3.9 at 15 T to 6 at 16 T. This clearly indicates the loss of the second subband to the dephasing processes and explains the fast increase of the dephasing time from 15 to 16 T. After 16 T, although the first pulse populates more carriers to the lowest subband with increasing magnetic field due to the density-dependent band gap shift, the rate of change becomes smaller as the lowest subband is nearly filled. However, the depopulation due to the second pulse becomes stronger with increasing magnetic fields. This can be seen from the fact that N_0/N_1 after the second pulse goes down from 6 for $B = 15$ T to finally 5 for $B = 20$ T. Our results show that the decrease of Pauli blocking together with the increasing of intra-subband scattering matrix element in the lowest subband dominate in the high magnetic field range the dephasing and explain the resulting decrease of dephasing time.

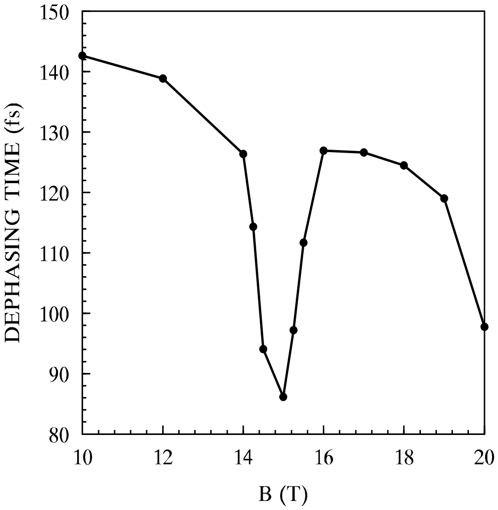

FIG. 9. Dephasing time as a function of B.

IV. COMPARISON WITH QUANTUM KINETIC CALCULATION

Because of the assumed pulse duration of 50 fs is already shorter than period of our quantum beats $T_c = 2\pi/(2\omega_c) = 119.7$ fs at $B = 10$ T, one may expect that the memory effects of the quantum kinetic scattering integrals already may play a role. Therefore we performed also quantum kinetic calculation based on Eqs. (12) and (15). In this case, there is an undetermined damping Γ in the memory kernel. In principle this term should be function of k, q, the magnetic field and the electron distributions, and should be determined self-consistently.[19] However, the inclusion of such effects will complicate the quantum kinetics considerably. Therefore, we took Γ as an adjustable constant. Such a simple approximation causes the violation of energy conservation in longtime limit and we find that the results, particularly for the TI FWM signals and therefore the dephasing are highly sensitive to the actual value of the damping constant.

In Fig. 10 we plot the TR FWM signal for pulses with $\chi = 0.3$ and $\tau = 240$ fs for $B = 18$ T. The solid curve is based on quantum kinetics with $\Gamma = 1.32$ meV. The dashed curve is the prediction based on Boltzmann kinetics as shown in Fig. 8(b). From Fig. 10 one can see that the two theories give qualitatively similar TR FWM signals, although the coherence of the polarization components is clearly larger according to quantum kinetics in the first few hundred femtoseconds because of the retarded onset of the dephasing processes in this theory.

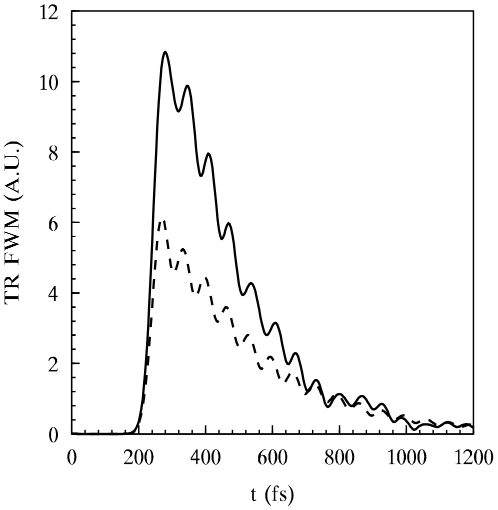

FIG. 10. TR FWM for pulses with $\chi = 0.3$ and delay $\tau = 240$ fs. $B = 18$ T. Solid curve: quantum kinetic result; Dashed curve: Boltzmann kinetics result.

However, we point out that the consistence in Fig. 10 depends on the choice of Γ and we failed to get consistent results for all the fields and delays with *one* constant damping Γ. A more detailed treatment of the damping of the memory kernel is needed for a consistent quantum kinetic theory.

V. CONCLUSION

In conclusion, we have performed theoretical studies of femtosecond kinetics of an optically excited 2D magnetoplasmas for intermediate- and high-density excitations. Based on a three-subband model in both the conduction and the valence band, our study is restricted to high magnetic fields. We calculated the intra- and inter-Landau-subband kinetics by bare Coulomb potential scattering and found pronounced relaxation oscillations to occur in the population of the two lowest Landau subbands for lower magnetic fields. We calculated both TR and TI FWM signals. Both signals exhibit quantum beats with frequencies around $2\omega_c$. Surprisingly, the resulting dephasing times are rather short and are modulated in the strong magnetic field by about 30%. Depending on the detuning of the laser pulses, the pulse width, the excited densities and the number of excited Landau subbands one gets decrease of the dephasing time with increasing B field because of the increase of the Coulomb matrix elements and the degeneracy of the Landau subbands. In regions where the loss of scattering channels exceeds these increasing effects, one can also obtain a slight increase of the dephasing time with the magnetic field. It is shown that the retarded onset of the dephasing and relaxation processes in quantum kinetics result in a FWM signal which is more coherent in the first few hundred femtoseconds. However a consistent theory of the decay of the memory kernel in a magneto-plasma is still missing. Finally, we point out that more Landau subbands are needed to account for the kinetics in lower magnetic fields. A corresponding extension of the theory is still under investigation and the results will be published elsewhere.

ACKNOWLEDGMENTS

We acknowledge financial support by the DFG within the DFG-Schwerpunkt “Quantenkohärenz in Halbleiter”. MWW would like to thank Prof. L. Bányai for valuable discussions during the initial stage of this work which helped him to get into this filed smoothly.

APPENDIX A:

We give the analytic expressions for all the Coulomb interaction matrix elements Eq. (8) up to the third Landau subbands. We first show the approximation we take in our calculation through $V_{00;00}$. After integrating out x and x', $V_{00;00}$ of Eq. (8) can be written into

$$V_{00;00} = \frac{e^2}{\epsilon_0} e^{-\frac{1}{2}\alpha^2\delta x_q^2 - \alpha^2\lambda^2(k-k')^2} \times \int_{-\infty}^{\infty} \frac{e^{-z^2}dz}{\sqrt{(z-i\alpha\lambda(k-k'))^2+q^2/(2\alpha^2)}} \; . \quad \text{(A1)}$$

Due to the factor $e^{-\alpha^2\lambda^2(k-k')^2}$ $V_{00;00}$ decays quickly with increasing $|k-k'|$. Therefore the main contribution to the matrix element comes from small values of $|k-k'|$. We therefore neglect the term $i\alpha\lambda(k-k')$ inside the integrand of Eq. (A1). The integral remaining can be carried out analytically. Similar approximation may be applied to other matrix elements and therefore, Eq. (8) may be written as

$$\begin{aligned} &V_{ni;jm}(q,k,k') \\ &\simeq \sum_{q_x} \frac{2\pi e^2}{\sqrt{q^2+q_x^2}} \int d(x_1x_2) e^{-iq_x(x_1-x_2)-\alpha^2\lambda^2(k-k')^2} \\ &\quad \times \phi_n^*(x_1+\delta x_q)\phi_i^*(x_2-\delta x_q)\phi_j(x_2)\phi_m(x_1) \; . \quad \text{(A2)} \end{aligned}$$

Defining two dimensionless variables $x = q^2/4m\Omega_x$ and $y = 2x\omega_c^2/\Omega_x^2$ as Ref. 11, one can express the matrix elements in terms of zeroth- (K_0) and first-order (K_1) modified Bessel functions. As there exist the following symmetry relations for the matrix elements

$$\begin{aligned} V_{ni;jm} &= V_{jm;ni} = (-1)^{n+m+i+j} V_{in;mj} \\ &= (-1)^{n+m+i+j} V_{mj;in} \; , \end{aligned} \quad \text{(A3)}$$

one only needs to calculate 27 terms. The remaining terms may be got from the symmetry relations. In the following we give these required 27 terms:

$$V_{00;00} = \frac{e^2}{\epsilon_0} e^{x-y-\Xi} K_0(x) \; ,$$

with $\Xi = \alpha^2\lambda^2(k-k')^2$.

$$V_{10;00} = -\frac{e^2}{\epsilon_0}\sqrt{y} e^{x-y-\Xi} K_0(x) \; .$$

It is noted here and hereafter the term $\sqrt{y}$ strictly should be $\sqrt{y}\mathrm{sgn}(q)$ with sgn standing for the sign function. However, due to the fact the all the terms with the factor $\sqrt{y}$ do not appear in the Hartree-Fock terms, we therefore just simplify it as $\sqrt{y}$.

$$V_{10;10} = \frac{e^2}{\epsilon_0} e^{x-y-\Xi}[(y-x)K_0(x) + xK_1(x)] \; ,$$

$$V_{11;00} = \frac{e^2}{\epsilon_0} e^{x-y-\Xi}[-(x+y)K_0(x) + xK_1(x)] \; ,$$

$$V_{10;01} = \frac{e^2}{\epsilon_0} e^{x-y-\Xi}[(1+x-y)K_0(x) - xK_1(x)] \; ,$$

$$V_{11;01} = \frac{e^2}{\epsilon_0} e^{x-y-\Xi}\sqrt{y}[(1+x+y)K_0(x) - xK_1(x)] \; ,$$

$$\begin{aligned} V_{11;11} = \frac{e^2}{\epsilon_0} e^{x-y-\Xi}\{&[1+2x+2x^2+y(y-2x-2)]K_0(x) \\ &+ x(2y-1-2x)K_1(x)\} \; , \end{aligned}$$

$$V_{20;00} = \frac{e^2}{\sqrt{2}\epsilon_0} e^{x-y-\Xi}[(x+y)K_0(x) - xK_1(x)] \; ,$$

$$V_{12;00} = -\frac{e^2}{\epsilon_0} e^{x-y-\Xi}\sqrt{y/2}[(3x+y)K_0(x) - 3xK_1(x)] \; ,$$

$$V_{02;01} = \frac{e^2}{\epsilon_0} e^{x-y-\Xi}\sqrt{y/2}[(y-x)K_0(x) + xK_1(x)] \; ,$$

$$V_{12;01}=\frac{e^2}{\sqrt{2}\epsilon_0}e^{x-y-\Xi}[(x+y+2x^2-y^2)K_0(x)-2x^2K_1(x)]\ ,$$

$$V_{02;02}=\frac{e^2}{\epsilon_0}e^{x-y-\Xi}[(\frac{1}{2}y^2-xy+x^2)K_0(x)+(xy+\frac{1}{2}x-x^2)K_1(x)]\ ,$$

$$V_{00;22}=\frac{e^2}{\epsilon_0}e^{x-y-\Xi}[(\frac{1}{2}y^2+3xy+x^2)K_0(x)+(\frac{1}{2}x-x^2-3xy)K_1(x)]\ ,$$

$$V_{20;21}=\frac{e^2}{\epsilon_0}e^{x-y-\Xi}\sqrt{y}[(\frac{1}{2}y^2+x^2+x-y-xy)K_0(x)+(xy-\frac{1}{2}x-x^2)K_1(x)]\ ,$$

$$V_{10;22}=-\frac{e^2}{\epsilon_0}e^{x-y-\Xi}\sqrt{y}[(\frac{1}{2}y^2-3x-y+xy-3x^2)K_0(x)+(3x^2-xy+\frac{3}{2}x)K_1(x)]\ ,$$

$$V_{22;20}=\frac{\sqrt{2}e^2}{\epsilon_0}e^{x-y-\Xi}[(\frac{1}{4}y^3-\frac{1}{4}xy^2-\frac{1}{2}x^2y+x^3-y^2+\frac{7}{4}x^2+\frac{1}{2}x)K_0(x)+(\frac{1}{4}xy^2+\frac{1}{2}x^2y-x^3-\frac{1}{4}xy-\frac{5}{4}x^2)K_1(x)]\ ,$$

$$V_{20;01}=\frac{e^2}{\epsilon_0}e^{x-y-\Xi}\sqrt{\frac{y}{2}}[(y-x-2)K_0(x)+xK_1(x)]\ ,$$

$$V_{12;10}=\frac{e^2}{\sqrt{2}\epsilon_0}e^{x-y-\Xi}[(y^2-2y-2x-2x^2)K_0(x)+(x+2x^2)K_1(x)]\ ,$$

$$V_{02;11}=-\frac{e^2}{\sqrt{2}\epsilon_0}e^{x-y-\Xi}[(y^2-2xy+2x^2+2x-2y)K_0(x)+(2xy-2x^2-x)K_1(x)]\ ,$$

$$V_{11;21}=\frac{e^2}{\epsilon_0}e^{x-y-\Xi}\sqrt{\frac{y}{2}}[(3y-3x-2-y^2+2xy-2x^2)K_0(x)-(2xy-2x^2-2x)K_1(x)]\ ,$$

$$V_{11;22}=-\frac{e^2}{\epsilon_0}e^{x-y-\Xi}\{[\frac{1}{2}(y-2)(y^2-2y-2x-xy-2x^2)+\frac{3}{2}x^2+2x^3]K_0(x)+(\frac{1}{2}xy^2+x^2y-\frac{1}{2}xy-x-2x^3-\frac{5}{2}x^2)K_1(x)\}\ ,$$

$$\begin{aligned}V_{21;22}=\frac{e^2}{\epsilon_0}e^{x-y-\Xi}\sqrt{2y}[&(\frac{1}{4}y^3-\frac{3}{2}y^2+3xy+\frac{3}{2}x^2y-\frac{3}{4}xy^2+\frac{5}{2}y-\frac{5}{2}x-1-\frac{5}{2}x^2-2x^3)K_0(x)\\&+[x^3+\frac{3}{4}y^2x-\frac{3}{2}x^2y-\frac{9}{4}xy+\frac{3}{2}x+\frac{9}{4}x^2)K_1(x)]\ ,\end{aligned}$$

$$V_{02;20}=\frac{e^2}{\epsilon_0}e^{x-y-\Xi}[(1+2x-2y-xy+x^2+\frac{1}{2}y^2)K_0(x)+(xy-x^2-\frac{3}{2}x)K_1(x)]\ ,$$

$$V_{12;20}=-\frac{e^2}{\epsilon_0}e^{x-y-\Xi}\sqrt(y)[(1+2x-2y-xy+x^2+\frac{1}{2}y^2)K_0(x)+(xy-x^2-\frac{3}{2}x)K_1(x)]\ ,$$

$$\begin{aligned}V_{12;21}=\frac{e^2}{\epsilon_0}e^{x-y-\Xi}[&(1+3x-3y-5xy+\frac{5}{2}y^2+\frac{9}{2}x^2-\frac{1}{2}y^3+2x^3-3x^2y+\frac{3}{2}xy^2)K_0(x)\\&+(-\frac{3}{2}x+\frac{7}{2}xy-\frac{7}{2}x^2-2x^3-\frac{3}{2}xy^2+3x^2y)K_1(x)]\ ,\end{aligned}$$

$$
\begin{aligned}
V_{21;21} = \frac{e^2}{\epsilon_0} e^{x-y-\Xi} [& (\frac{1}{2}y^3 - 2y^2 + 2y - \frac{3}{2}xy^2 + 4xy - 2x + 3x^2y - \frac{7}{2}x^2 - 2x^3)K_0(x) \\
& + (\frac{3}{2}xy^2 - \frac{5}{2}xy - 3x^2y + x + 2x^3 + \frac{5}{2}x^2)K_1(x)] \ ,
\end{aligned}
$$

$$
\begin{aligned}
V_{22;22} = \frac{e^2}{\epsilon_0} e^{x-y-\Xi} [& (\frac{1}{4}y^4 - 4x^3y + 3x^2y^2 + 2x^4 - xy^3 - 2y^3 + 6xy^2 - 11x^2y + 7x^3 + 5y^2 - 10xy + \frac{35}{4}x^2 - 4y \\
& + 4x + 1)K_0(x) + (xy^3 - 3x^2y^2 + 4x^3y - 2x^4 - \frac{9}{2}xy^2 + 9x^2y - 6x^3 + 6xy - 6x^2 - \frac{3}{2}x)K_1(x)] \ .
\end{aligned}
$$

---

[1] Proceedings of the Third International Workshop on Nonlinear Optics and Excitation Kinetics in Semiconductors, Bad Honnef, Germany [Phys. Stat. Sol. B **173**, 11 (1992)].

[2] J. Shah, *Ultrafast Spectroscopy of Semiconductors and Semiconductor Microstructures* (Springer, Berlin, 1996).

[3] H. Haug and A.P. Jauho, *Quantum Kinetics in Transport and Optics of Semiconductors* (Springer, Berlin, 1996).

[4] C. Stafford, S. Schmitt-Rink, and W. Schaefer, Phys. Rev. B **41**, 10000(1990).

[5] S. Glutsch and D.S. Chemla, Phys. Rev. B **52**, 8317 (1995).

[6] U. Siegner, S. Bar-Ad, and D.S. Chemla, Chem. Phys. **210**, 155 (1996).

[7] T. Rappen, G. Mohs, and M. Wegener, Appl. Phys. Lett. **63**, 1222 (1993).

[8] Q.T. Vu, L. Bányai, P.I. Tamborenea, and H. Haug, Europhys. Lett. **40**, 323 (1997).

[9] G.E.W. Bauer, Phys. Rev. Lett. **64**, 60 (1981) and Phys. Rev. B **45**, 9153 (1993).

[10] Private communications by D.S. Chemla and H. Roskos.

[11] M. Bayer *et al.*, Phys. Rev. B **55**, 13180 (1997).

[12] M. Benisty, C.M. Sotomayor-Torrès, and C. Weisbuch, Phys. Rev. B **44**, 10945 (1991).

[13] T. Rappen, G. Mohs, and M. Wegener, Appl. Phys. Lett. **63**, 1222 (1993).

[14] W. Braun *et al.*, Phys. Rev. B **57**, 12364 (1998).

[15] J. Callaway, *Quantum Theory of the Solid State*, 2nd ed. (Academic, San Diego, 1991), Chap. 6.

[16] L. Bányai, E. Reitsamer, and H. Haug, J. Opt. Soc. Am. B **13**, 1278 (1996).

[17] M. Lindberg, R. Binder, and S.W. Koch, Phys. Rev. A **45**, 1865 (1996).

[18] K. Leo *et al.*, Phys. Rev. B **44**, 5726 (1991).

[19] H. Haug and L. Bányai, Sol. Stat. Comm. **100**, 103 (1996); L. Bányai, H. Haug, and P. Gartner, Europ. Phys. J. B **1**, 209 (1998).